

Estimating the Influence of Evaporation and Moisture-Flux Convergence upon Seasonal Precipitation Rates. Part II: An Analysis for North America Based upon the NCEP–DOE Reanalysis II Model

BRUCE T. ANDERSON

Department of Geography and Environment, Boston University, Boston, Massachusetts

ALEX C. RUANE

NASA Postdoctoral Program, Oak Ridge Associated Universities, Oak Ridge, Tennessee, and NASA Goddard Institute for Space Studies, New York, New York

JOHN O. ROADS AND MASAO KANAMITSU

Scripps Institution of Oceanography, University of California, San Diego, La Jolla, California

(Manuscript received 9 June 2008, in final form 27 February 2009)

ABSTRACT

In this paper, a diagnostic metric—termed the *local-convergence ratio*—is used to analyze the contribution of evaporation and atmospheric moisture-flux convergence to model-based estimates of climatological precipitation over the North American continent. Generally, the fractional evaporative contribution is largest during spring and summer when evaporation is largest and decreases as evaporation decreases. However, there appears to be at least three regions with distinct spatiotemporal seasonal evolutions of this ratio. Over both the northern and western portions of the continent, the fractional evaporative contribution peaks in spring and early summer and decreases during fall and into winter. Over the northern portion, this fall decrease is related to an increase in atmospheric moisture-flux convergence associated with enhanced meridional moisture fluxes into the region; over the western coastal regions, the fall decrease in evaporative contribution is associated with a decrease in evaporation and an increase in total moisture-flux convergence, most likely associated with increased storm activity. In contrast, over the central portions of the continent, the fractional evaporative contribution to precipitation remains relatively low in spring—when enhanced low-level jet activity increases the low-level atmospheric moisture flux convergence into the region—and instead peaks in summer and fall—when the moisture-flux convergence associated with the low-level jet decreases and precipitation is balanced predominantly by local evaporation. Finally, over the southwestern United States and northwestern Mexico, the fractional evaporative contribution to precipitation is found to contain a wintertime minimum as well as a secondary minimum during summer. This latter feature is due to a substantial increase in low-level atmospheric moisture-flux convergence associated with the large-scale monsoon circulation that influences this region during this time.

1. Introduction

North America is one of the best meteorologically and climatologically monitored regions in the world, and its distinct regional characteristics make it an ideal test bed for hydrometeorological analyses. One of the

earliest to look at atmospheric hydrologic balances across the region was Rasmusson (1968). Since then, major hydroclimatic studies of the region include the Global Energy and Water Cycle Experiment (GEWEX) Americas Prediction Project (GAPP) over the Mississippi River basin (Roads et al. 2003), the Mackenzie GEWEX Study (MAGS; Stewart et al. 1998), and the North American Monsoon Experiment (Higgins et al. 2006). Generally, the hydroclimate of the Pacific Coast, from California to Alaska, is controlled by the seasonal track of synoptic storms that interact with steep mountain ranges (see, e.g.,

Corresponding author address: Bruce T. Anderson, Boston University, 675 Commonwealth Ave., Rm. 457, Boston, MA, 02215-1401.
E-mail: brucea@bu.edu

Ruane and Roads 2008). In contrast, over the southwestern U.S. interior and northwestern Mexico, a strong monsoonal circulation dominates the hydroclimate, resulting in dry winters and wet summers (Douglas et al. 1993). To the east over the Great Plains, precipitation tends to be low (when compared with the western and eastern coastal regions), particularly during winter, as dry air descends into the region from the Rocky Mountain plateau; however, in spring and summertime a strong low-level jet draws moisture into the continental interior from the Gulf of Mexico (Higgins et al. 1997b), feeding convective storms as they propagate from the lee of the Rocky Mountains to the Great Lakes (Carbone et al. 2002) and producing a peculiar nocturnal maximum in diurnal precipitation in the upper Midwest (Wallace 1975). Over the eastern third of the continent, there are generally higher rainfall totals with weak seasonal variation, although large interannual variability is influenced by the El Niño/Southern Oscillation (Ropelewski and Halpert 1986) and the North Atlantic Oscillation (Hurrell and van Loon 1997).

Given the complexity of these various processes, researchers have turned to numerical modeling systems to diagnose important hydroclimatological mechanisms that link changes in atmospheric water vapor, precipitation, and evaporation in different regions (e.g., Roads et al. 1992; Chen et al. 1996; Higgins 1996; Maurer et al. 2001; Roads et al. 2003). The data from these modeling systems can be combined in various ways to help analyze and diagnose the complexity of the hydrologic components. For example, by treating the seasonal values of evaporation, vertically integrated moisture-flux convergence, and precipitation as sources/sinks of moisture, Kanamitsu (2003) was able to compare the relationships between the various sources/sinks and categorize three main types of hydrologic balances. In the first category, there are positive correlations between anomalies in evaporation/convergence, evaporation/precipitation, and precipitation/convergence. The other two prominent categories involve 1) negative evaporation/convergence and evaporation/precipitation correlations but positive precipitation/convergence correlations and 2) negative evaporation/convergence and convergence/precipitation correlations but positive evaporation/precipitation correlations. Similarly, Ruane and Roads (2008) examined the normalized covariances between the sources/sinks of moisture at various frequencies and found significant regional variations in the dominant balances and exchanges at intra-annual, intraseasonal, and diurnal time scales. Using these correlations and covariances as a guide, it is then possible to identify specific processes (e.g., increased soil moisture, enhanced

convection, and so forth) that link one source/sink with another.

One drawback of the approach described above is that correlation/covariance statistics alone simply capture the linear relation between the fields (for instance, increased precipitation leading to increased soil moisture, resulting in excess evaporation) and may not necessarily capture nonlinear relations between the fields, which might be indicative of feedback effects. Previous efforts have attempted to describe feedback processes through the introduction of a regional moisture recycling metric referred to as the precipitation-recycling ratio ρ (Brubaker et al. 1993; Burde and Zangvil 2001; Bosilovich and Schubert 2002). This ratio is defined as the fraction of total precipitation (P) that is composed of precipitation of evaporative (or “local”) origin (P_l):

$$\rho \equiv \frac{P_l}{P}. \quad (1)$$

To estimate this ratio, most methods depend upon the assumption that the ratio of locally derived precipitation to total precipitation is the same as the ratio of locally derived precipitable water to total precipitable water (Burde and Zangvil 2001). In this context, locally derived precipitation (P_l) is defined as the fraction of water molecules rained out within a given region that originated from within the region via evaporation—that is, it quantifies the local contribution of mass available for precipitation.

In a previous paper (Anderson et al. 2008), a second metric is introduced—termed the *local-convergence ratio*—for estimating the fraction of the time-mean precipitation rate (or budget) that is balanced by convergence of moisture via evaporation (compared with the precipitation rate that is balanced by moisture-flux convergence). As such, this ratio is designed to quantify the local contribution to the atmospheric moisture budget within a given region that, in turn, can balance time-mean precipitation rates within the same region, even if the actual water molecules that precipitate out come from another region.

A full derivation and explanation of this new ratio is provided in Anderson et al. (2008); here, we provide a brief overview. If we define the operator $\{\dots\}$ as

$$\{\dots\} = \pi \int_1^0 \dots d\sigma, \quad (2)$$

where $\sigma = p(z)/p_s$ and $\pi = p_s/g$, and where $p(z)$ is the pressure at a given height (level), p_s is the surface pressure, and g is the gravitational constant; then, the vertically integrated tendency equation for specific humidity (q) becomes (Starr and Peixoto 1958)

$$\frac{\partial\{q\}}{\partial t} + \nabla \cdot \{\mathbf{u}q\} = E - P. \quad (3)$$

Key to the derivation of the new metric is the recognition that the vertically integrated net moisture-flux divergence, $\nabla \cdot \{\mathbf{u}q\}$, can be partitioned into the total moisture-flux convergence (χ) and the total moisture-flux divergence (δ). These are defined as the sum of the *horizontal* moisture-flux convergence/divergence only at levels that have positive values:

$$\chi \equiv \sum_{\sigma} -(\nabla \cdot \mathbf{Q}) \times H(-\nabla \cdot \mathbf{Q}) \quad \text{and} \quad (4)$$

$$\delta \equiv \sum_{\sigma} (\nabla \cdot \mathbf{Q}) \times H(\nabla \cdot \mathbf{Q}), \quad (5)$$

where $\nabla \cdot \mathbf{Q} \equiv \nabla_H \cdot \pi \mathbf{u}q|d\sigma|$ is the 2D horizontal moisture-flux divergence at a given sigma level and $H(x)$ is the Heaviside step function [where $H(x) = 1$ for $x > 0$ and $H(x) = 0$ for $x < 0$].

Since the vertical sum of the vertical moisture-flux divergence term $[(\partial\pi\sigma q)/\partial\sigma]$ is 0 when integrating through the entire atmospheric column and given that on climatological time scales (i.e., longer than 10–15 days) the local tendency term is near zero (Roads et al. 2002), it can be shown that

$$P + \delta = E + \chi. \quad (6)$$

For this balance to hold, the time-averaging must first be applied to $\nabla \cdot \mathbf{Q}$, E , and P . From the time-averaged values of $\nabla \cdot \mathbf{Q}$, we can arrive at a value of χ and δ . Doing so accounts for “precursor” sources of atmospheric moisture—either from the underlying surface (in the form of evaporation) or from outside the region (via moisture flux convergence)—that can then feed precipitation via moisture withdrawal (e.g., via negative moisture tendency). In addition, it accounts for very large values of horizontal moisture-flux divergence/convergence on daily time scales—which contribute to local tendency but may not produce precipitation—that are subsequently balanced by moisture-flux convergence/divergence of similar magnitude but opposite sign on other days.

Returning to Eq. (6), this balance equation indicates that the area-average evaporation E [which has units of $\text{kg} (\text{m}^2 \text{s})^{-1}$ and represents a convergence of moisture into the atmospheric column] is augmented by total moisture-flux convergence (χ). Some of the moisture supplied by E and χ precipitates out (P); what does not precipitate out is removed via total moisture-flux divergence, δ . If we assume that the convergent moisture (i.e., as supplied by E and χ) is well mixed (via vertical moisture-flux convergence in conjunction with turbulent diffusion), then the proportion of precipitation

balanced by the local convergence of moisture (P_{lc}) and that balanced by moisture-flux convergence from outside the region (P_{fc}) are in the same ratio as the area-averaged evaporation (E) and the total moisture-flux convergence (χ).

Making the assumptions above allows us to write

$$P = P_{lc} + P_{fc} = \frac{E}{E + \chi} P + \frac{\chi}{E + \chi} P. \quad (7)$$

We then define the “local-convergence ratio,” λ , as

$$\lambda \equiv \frac{P_{lc}}{P} = \frac{E}{E + \chi}. \quad (8)$$

Although the local-convergence ratio and the recycling ratio have similar forms, it is important to emphasize that one (the local-convergence ratio) is a convergence-based estimate and one (the precipitation-recycling ratio) is a flux-based estimate. In addition, it is important to note here that although both ratios utilize estimates of evaporation to quantify local contributions to precipitable water/precipitation, evaporation in and of itself is not a precipitation-producing process. In this sense, evaporation, and the two metrics derived from evaporation, may provide limited information about the meteorological rainfall-producing *processes* that are acting within a region, which are also dependent upon factors such as shifts in the horizontal and vertical circulations of the atmosphere as well as instabilities in the thermodynamic profile. Instead, these metrics are designed to provide an estimate of the contribution of evaporation to the precipitable water and precipitation budget within a region on a climatological scale, not necessarily a synoptic scale.

Given the additional insight that may be provided by the local-convergence ratio, in this paper we will use it to examine the heterogeneous influence of local (and remote) moisture convergence upon seasonal precipitation rates and their evolution over the course of the annual cycle for the North American region. Section 2 will describe the datasets used to derive the metric for this study. Section 3 will examine results for different climate regimes over the North American continent. Section 4 will provide a summary and some discussion of these results.

2. Data and methods

a. Data

For this study, we will use 3 yr of 6-h model forecasts taken from the National Centers for Environmental Prediction–Department of Energy (NCEP–DOE) Reanalysis-2 model. A full description of these model

runs is provided in Ruane and Roads (2007a,b). Here we provide a brief overview. To perform these forecasts, the NCEP/DOE Reanalysis-2 model (R2; Kanamitsu et al. 2002) initialized with the NCEP-NCAR Reanalysis-2 data, along with a linear interpolation of weekly-mean sea surface temperature values, was used to produce augmented 6-h forecasts 4 times each day (at 0000, 0600, 1200, and 1800 UTC). This global model uses the primitive (prognostic) equations for virtual temperature, humidity, surface pressure, and momentum, resolved in the horizontal with spherical harmonics at a triangular truncation of 62 and in the vertical with 28 sigma levels. Output is provided every 3 h on a 192×94 Gaussian grid, with pixels approximately 1.9° across. The integrations from this model were carried out for the Coordinated Enhanced Observing Period (CEOP, 2002–04; Lawford et al. 2006). The precipitation and atmospheric hydrology diagnostics from these model runs have been evaluated in Ruane and Roads (2007a,b). Here we will utilize the relevant global T62 gridpoint data pertaining to the atmospheric hydrologic cycle (see below). For this research we will select only those land-based grid points between 10° – 60° N and 60° – 135° W, covering the subtropical, midlatitude, and subarctic regions of the North American continent.

b. Calculation of local-convergence ratio

For the local-convergence ratio [Eq. (8)], we need to estimate

$$\lambda \equiv \frac{P_{lc}}{P} = \frac{E}{E + \chi}.$$

The model outputs the time-average evaporation rate (E) for the 3-h integration period, which we will use here. We note that here and throughout the paper, “evaporation” will be used to represent the direct transfer of water from the land surface to the atmosphere via evaporation as well as the indirect transfer via transpiration, which is an important source of moisture to the atmosphere in many regions.

To estimate the total moisture-flux convergence term, χ , we archive the 3D moisture-flux divergence term at each sigma level, $DQ(\sigma)$, which the model outputs at the end of each 3-h integration. We also archive the mass-weighted vertical moisture fluxes ($\pi\sigma q$) at each level (which, like the 3D moisture-flux divergence values, are instantaneous values provided by the model as part of the output stream at the end of each 3-h integration). We then derive the vertical moisture-flux divergence term, $VDQ(\sigma)$, by taking the vertical derivative of $\pi\sigma q$. Subtracting this from the full 3D moisture-flux divergence term gives just the horizontal

moisture-flux divergence term for the given level, $HDQ(\sigma)$ (see Anderson et al. 2008 for details).

For the local-convergence ratio, we want an estimate of total moisture-flux convergence (χ), which we define as the sum of horizontal moisture-flux convergence only at levels that have positive values. Using the nomenclature in this subsection, Eq. (4) becomes

$$\chi \equiv \sum_{\sigma} -[HDQ(\sigma)|d\sigma] \times H[-HDQ(\sigma)]. \quad (9)$$

c. Time averaging

It is important to note that for the original balance to hold [Eq. (6)], we need to take a time average over a relatively long time period to make the assumption that the local tendency term is zero. For this paper we will adopt a 30-day averaging period to estimate the mean profiles for $HDQ(\sigma)$, as well as evaporation (E) and precipitation (P), at each grid point. To do so, a 30-day box filter, centered on each day, will be used to estimate the value of $HDQ(\sigma)$, E , and P for that day based upon the 3-h values available from the model simulation. From the 30-day mean value of $HDQ(\sigma)$, we can arrive at a value of χ for each day from Eq. (9); in addition, we can estimate λ for each day from Eq. (8). For monthly- and seasonal-mean values, we take the average of these 30-day mean values (E , P , χ , and λ) across the given time period. Although this introduces some information from outside the averaging time period, this averaging method effectively represents a trapezoidal-filter average weighted toward the center of the period under consideration. For climatological values, we average the 30-day mean values for a given day (or month/season) across the three years of output provided by the model simulation. In addition, where appropriate, as a qualitative way of determining consistency, we also provide the minimum and maximum values of the given quantity (since three years is deemed too short a period to provide a true estimate of the error of the mean). Although we choose a 30-day averaging period for this study, sensitivity analyses (not shown) indicate that values of χ are quantitatively similar (within 20%) when using averaging periods between 20 and 60 days, as are estimates of the local-convergence ratios, λ (which are generally within 10% when using averaging periods between 20 and 60 days).

d. Rotation of principal components

The analysis in section 2c allows us to examine the gridpoint structure of the local convergence ratio and its respective hydrologic components. To determine the large-scale spatial patterns of the local-convergence ratio and the seasonal evolution of these patterns, we

compute a singular value decomposition (SVD) of the climatological annual evolution of the daily 30-day mean local-convergence ratio at each grid point, weighted by the square root of the area. To further distinguish the spatial and temporal patterns within each dataset, a Varimax rotation is performed (Richman 1986), which we apply to the spatial principal components (PCs). To calculate the temporal loadings, the rotated spatial patterns, which represent weighted components, are divided by the gridpoint standard deviations of the corresponding anomaly field to arrive at correlation coefficient values. Then the normalized spatial pattern is spatially correlated with the original (weighted) anomaly field to compute the temporal component. The resulting time series are normalized such that their inner products are unity. The rotation of the principal components, as done here, preserves orthogonality of the components in space but does not necessarily preserve orthogonality of the associated time series. Although these time series are not orthogonal (as they would be if we performed the rotation on the time series represented by the eigenvectors), we chose to do this rotation because it does not introduce artificial time series behavior needed to maintain this orthogonality. In addition, although neither the spatial nor temporal patterns represent a weighted fields per se, we still will refer to the spatial patterns as the rotated PCs and the time series as the associated eigenvectors.

For the figures showing the spatial patterns, only correlation coefficients greater than ± 0.3 will be presented. Because the seasonal evolution of the local-convergence ratios have intrinsic autocorrelation, following Ebisuzaki (1997) we test explicitly for significance of these values by performing a modified bootstrap analysis using randomized versions of each 30-day mean gridpoint time series. These randomized gridpoint time series are produced by randomizing the *phase* of the associated power spectra and then reconstructing the time series using the amplitudes; in this way, the gridpoint autocorrelation structure is preserved but the time series is randomized with respect to other grid points. We then perform the rotated-SVD procedure upon the randomized gridpoint time series; this randomization is repeated 1000 times. Based upon this analysis, we find $|r| = 0.15$ is above the 99% confidence interval at all grid points, suggesting that values presented in the figures are statistically significant.

3. Results

Figure 1 shows maps of the seasonal-mean local-convergence ratio for boreal spring (March–May), summer (June–August, JJA), fall (September–November),

and winter (December–February) over North America. The hydrologic components that comprise the local-convergence ratio— E and χ , respectively—are shown in Figs. 2, 3.

Generally, local-convergence ratios are smaller during fall and winter than during spring and summer, primarily the result of a decrease in evaporation during the former two seasons (Fig. 2). During spring (Fig. 1a), local-convergence ratios are fairly high along the western interior portion of the United States extending into most of Canada. Ratios are also high over the southeastern United States where evaporation is largest (Fig. 2a). In contrast, a local minimum extends from central Mexico along the western Great Plains states, where the total moisture-flux convergence term is a maximum (Fig. 3a), and into the Great Lakes region. We will show that the minimum in the local-convergence ratio over the western Great Plains region is related to intensified low-level convergence of moisture that accompanies the springtime enhancement of the low-level jet in this region (Higgins 1996; Ruane and Roads 2007a). In addition, there are local minima in the local-convergence ratios along the western coast of North America. Although evaporation here is larger than over the western interior (Fig. 2a), so too is the total moisture-flux convergence (Fig. 3a), indicating relatively large remote contributions to precipitation in these regions.

During summer (Fig. 1b), values of the local-convergence ratio are high across most of North America, as evaporation rates increase during the high-sun period (Fig. 2b). Relatively low values are still found over the western coastal regions of Canada as well as over the foothill regions to the east of the Rocky Mountains. The lowest values are found over western Mexico, with a tongue of relatively low values extending into New Mexico and parts of Arizona. During this time, the total moisture-flux convergence values are largest over western Mexico (Fig. 3b); these high total moisture-flux convergence values extend into the southwestern United States and along the foothills of the Rocky Mountain plateau. We will show that in these regions, the onset of the summertime North American monsoon circulation over northern Mexico and the southwestern United States produces an increase in low-level moisture-flux convergence that supports summertime precipitation during this time (Higgins et al. 1997a; Anderson and Roads 2001).

During fall (Fig. 1c), local-convergence ratios tend to be low over the western portion of North America and relatively higher over the eastern portion. This pattern matches the pattern of evaporation, with relatively low values over the western half of the domain and elevated values over the eastern portion of the continent (Fig. 2c).

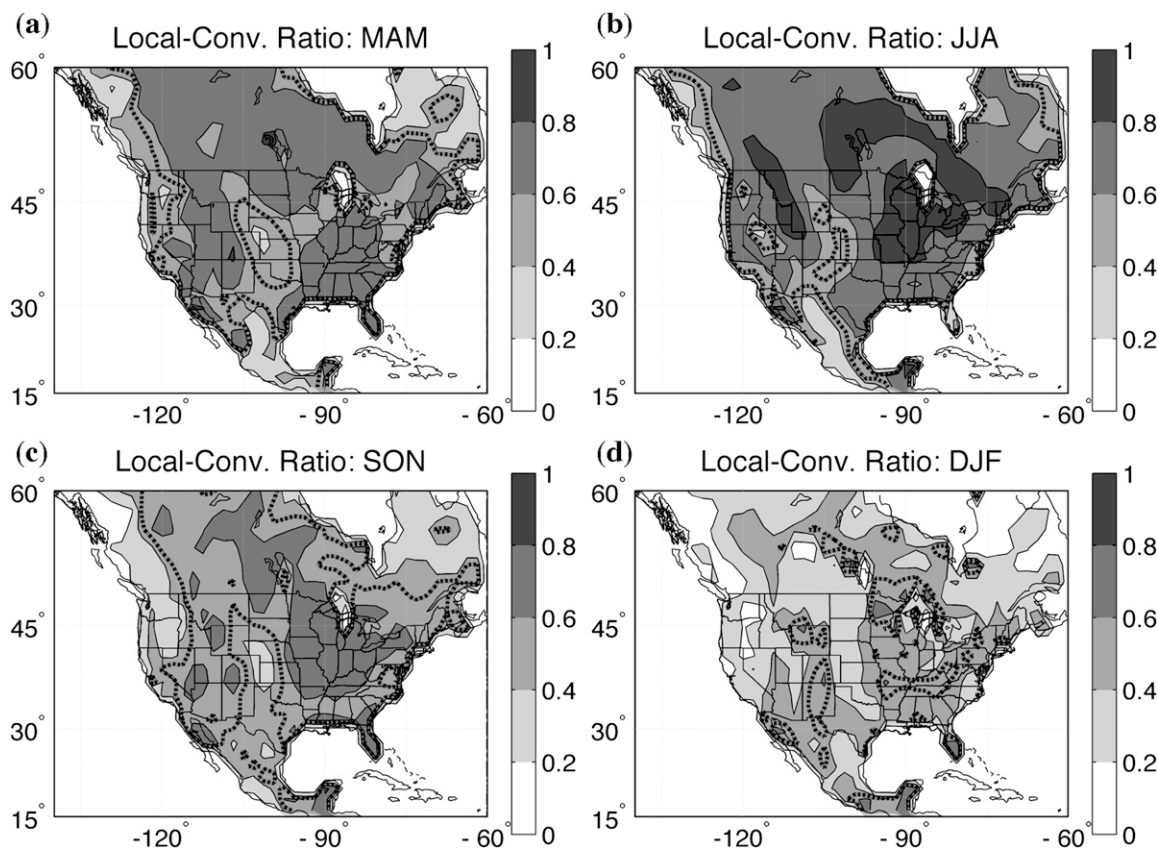


FIG. 1. (a) Seasonal-mean local-convergence ratio for March–May derived from Eq. (8). Estimates based upon 3-month averages of evaporation and χ . Data derived from 3-h integrations of the RII atmospheric model. Contour and shading interval is 0.2; thick dashed line indicates $\lambda = 0.5$ value. (b) Same as (a) but for June–August. (c) As in (a), but for September–November. (d) As in (a), but for December–February.

The lowest local-convergence ratios during this time are found along the northwestern coastal regions, principally related to increased total moisture-flux convergence values (Fig. 3c).

During winter (Fig. 1d), local-convergence ratios are generally smaller than at any other time, largely because of the decrease in evaporation during the low-sun season (Fig. 2d). There is no strong regional signature to the patterns; although, there is some indication that east of the Rocky Mountain plateau there is a local minimum in the ratio, related to local maxima in the total moisture-flux convergence (Fig. 3d). In addition, there are local maxima in the total moisture-flux convergence along the west coast of the United States (Fig. 3d), which contribute to local minima in the local-convergence ratios in these regions (Fig. 1d).

For comparison, Fig. 4 shows maps of a traditional measure of the recycling ratio (Brubaker et al. 1993) for boreal spring (March–May), summer (June–August), fall (September–November), and winter (December–February) over North America. Qualitatively, this method

compares the vertically integrated fluxes of moisture into a region with the fluxes via evaporation along a parcel trajectory length, which we set to 500 km, as in Trenberth (1999); see Anderson et al. (2008) for details. Generally, the recycling ratio indicates lower values in mid-to-high latitudes during hemispheric winter and higher values during hemispheric summer, in agreement with traditional estimates taken from longer-term climatological values (Trenberth 1999) and more sophisticated back-trajectory analyses (Dirmeyer and Brubaker 2007). However, the traditional flux-based recycling ratio tends to be smaller than the local-convergence ratio (see Fig. 1), particularly during hemispheric winter, suggesting that local evaporation may have a more prominent role in contributing to seasonal precipitation rates than is implied by recycling ratios. One exception to this generalization appears to be over the southwestern United States and northwestern Mexico during boreal summer. During this period, this region sits near the center of the monsoon circulation; hence, horizontal moisture fluxes weaken considerably (Higgins et al.

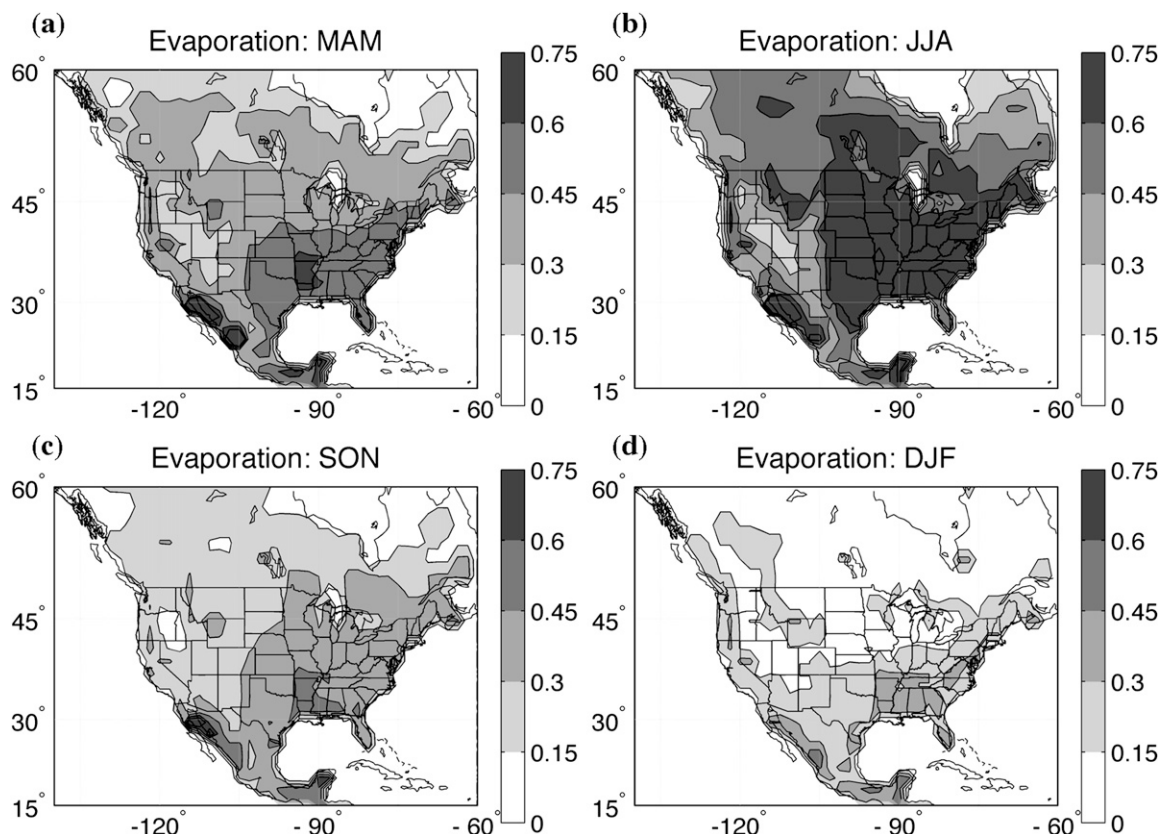


FIG. 2. (a) Seasonal-mean evaporation rate ($10^{-4} \text{ kg m}^{-2} \text{ s}^{-1}$) for March–May. Data derived from 3-h integrations of the RII atmospheric model. (b) Same as (a) but for June–August. (c) As in (a), but for September–November. (d) As in (a), but for December–February.

1997a; Anderson and Roads 2001), resulting in higher values for the precipitation-recycling ratio (Fig. 4b). For a more comprehensive analysis of the difference between the two metrics and their relation to the corresponding moisture fluxes and moisture-flux convergence terms—both for regions over North America and over other portions of the globe—see Anderson et al. (2008).

a. Rotated principal components

As discussed in section 2, to examine the large-scale features of the seasonal evolution of the local-convergence ratio, we perform a rotation of the spatial principal components derived from an SVD of the area-weighted climatological 30-day mean local-convergence ratio time series. For this study, we select the first three spatial principal components, weighted by their eigenvalues to maintain variance associated with each spatial pattern; these components capture 85% of the variance of the full dataset. This procedure allows us to identify spatial patterns with coherent seasonal evolution as well as the corresponding time series (Fig. 5). We note here

that the same leading three spatial patterns are produced when including more principal components into the algorithm; the additional higher-order rotated patterns simply capture additional finescale features across the domain (not shown).

The first pattern (Fig. 5a) is associated with the seasonal evolution of the local-convergence ratio over the northwestern portion of the United States, along with most of Canada. The related time series indicates these regions have minimum local-convergence ratios during fall and winter, with an increase in March, leading to maximum values in late spring and throughout summer.

The second pattern (Fig. 5c) is associated with the seasonal evolution over the Great Plains region to the east of the Rocky Mountains, extending into the Great Lakes region. The associated time series indicates this pattern also has minimum values in winter; however, these minimum values extend through most of spring (Fig. 5d). Peak values are found during summer and early fall. Hence the seasonal pattern is shifted later in the year compared with regions to the west and north (as seen in the first pattern).

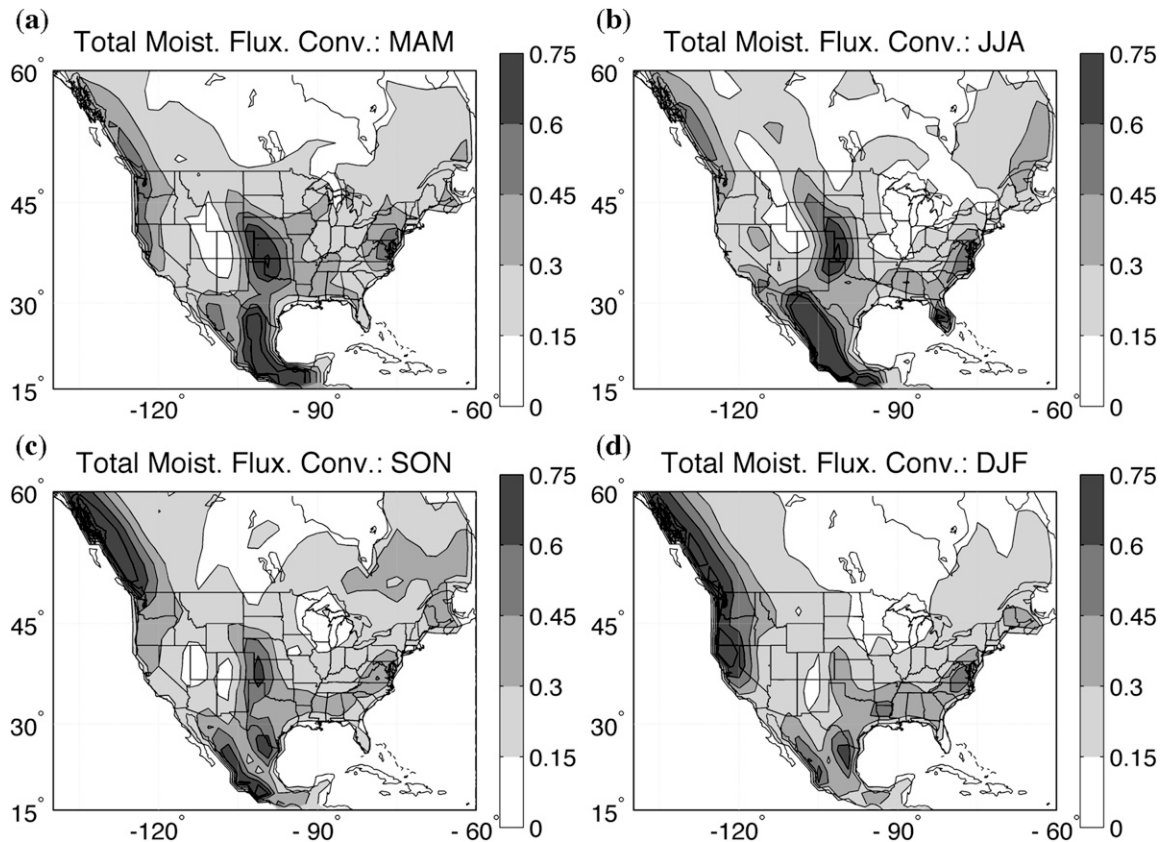


FIG. 3. (a) Seasonal-mean χ ($10^{-4} \text{ kg m}^{-2} \text{ s}^{-1}$) for March–May. Data derived from 3-h integrations of the RII atmospheric model. Units are. (b) As in (a), but for June–August. (c) As in (a), but for September–November. (d) As in (a), but for December–February.

The third pattern (Fig. 5e) is associated with the seasonal evolution over the southwestern portion of the United States and the northwestern portion of Mexico. The related time series shows minimum values during the early winter season. In addition, there is also a local minimum centered on July and August, the period of active monsoon rainfall in this region (e.g., Comrie and Glenn 1998).

Because the time series of rotated PCs tend to represent an amalgamation of the seasonal evolution of the grid points that make up the spatial pattern, here we select representative grid points for each spatial pattern, shown as black circles on each map. Using these grid points, we will analyze the seasonal evolution of the local-convergence ratio as well as the important hydrologic components—including evaporation, precipitation, and total moisture-flux convergence—to identify how they contribute to the seasonal evolution seen in the rotated principal component time series. It should be noted that similar analyses have been performed on representative area-averaging regions and all results are qualitatively similar (not shown).

b. First rotated principal component pattern

For the first spatial pattern (rotated PC1), we choose two grid points—one in central Canada and one over the northwestern coast of North America—because they have similar evolutions in their local-convergence ratios but for different reasons (as will be highlighted below). Over central Canada, the seasonal evolution of the hydrologic components indicates a relatively rapid rise in evaporation with a short-lived maximum, followed by a rapid decrease through fall (Fig. 6a). Precipitation also increases with evaporation. However, precipitation remains high through fall even as the evaporation term decreases. This persistence of precipitation appears to be balanced by an increase in total moisture-flux convergence during this time. During winter, both the total-convergence term and the evaporation term decrease significantly, as does precipitation. Examining the local-convergence ratio for this grid point (Fig. 6b), minimum values are found during winter with a slow increase through spring, leading to maximum values during the early and midsummer

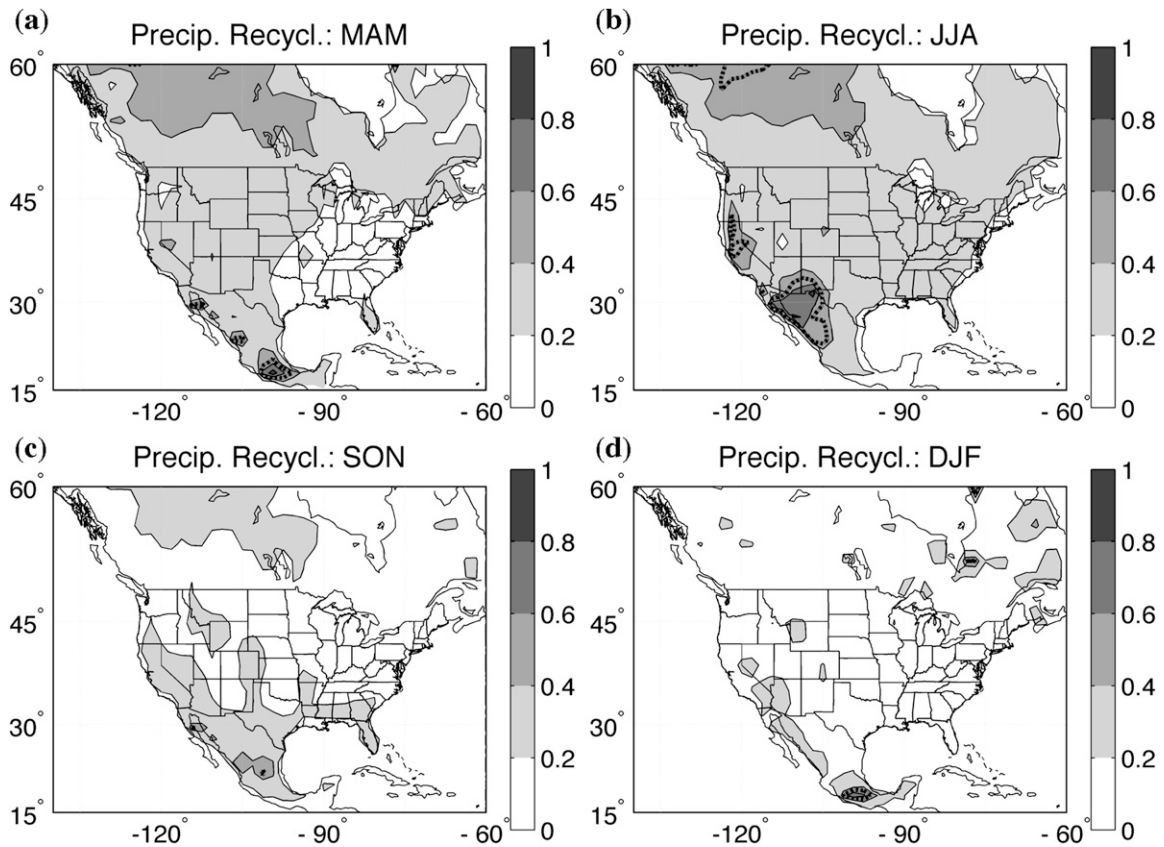


FIG. 4. (a) Seasonal-mean precipitation-recycling ratio for March–May derived from Brubaker et al. (1993). Estimates based upon 3-month averages of evaporation and vertically integrated moisture fluxes for the respective months. Length scale, L , is 500 km. Data derived from 3-h integrations of the RII atmospheric model. Contour and shading interval is 0.2; thick dashed line indicates $\rho = 0.5$ value. (b) As in (a), but for June–August. (c) As in (a), but for September–November. (d) As in (a), but for December–February.

season. The values then drop starting in September and decay through the rest of fall into winter. Overall, this evolution suggests that fall and winter precipitation are balanced more by moisture-flux convergence, relative to spring and summer when most of the precipitation is balanced by local evaporation.

Next, we look at the actual amount of precipitation balanced by the local convergence of moisture (P_{lc}) and that balanced by moisture-flux convergence from outside the region (P_{fc} ; Fig. 7). Here, P_{lc} is determined for each year and each day by multiplying the 30-day running mean local-convergence ratio, λ , by the 30-day running mean precipitation amount, P , for the given day (results here and below are quantitatively the same if we instead calculate the climatological mean of λ and P for the given day and then find their product—not shown); P_{fc} is the difference between P_{lc} and P . Because there are year-to-year variations in both the overall precipitation amounts, as well as in the fractional contribution supported by local precipitation (as given by

the local-convergence ratio), for this figure we only calculate the range of values using the year-to-year variations in the local-convergence ratio, applied to the climatological precipitation values, to better understand whether these show consistency across all three years. We find that although moisture-flux convergence contributes more to the fall and winter precipitation budgets, the low overall precipitation during this time means that moisture-flux convergence does not contribute much to the overall annual precipitation budget. Instead the predominant contribution to annual precipitation is through local evaporation, principally during summer. We can quantify the contribution by calculating the fractional amount of annual precipitation contributed by the annual values of P_{lc} and P_{fc} (Table 1); results indicate that the local contribution of evaporation to overall annual precipitation is about 66%. Previous results, based upon the column-integrated water cycle, also found that evaporation was the primary supply of precipitating moisture in the

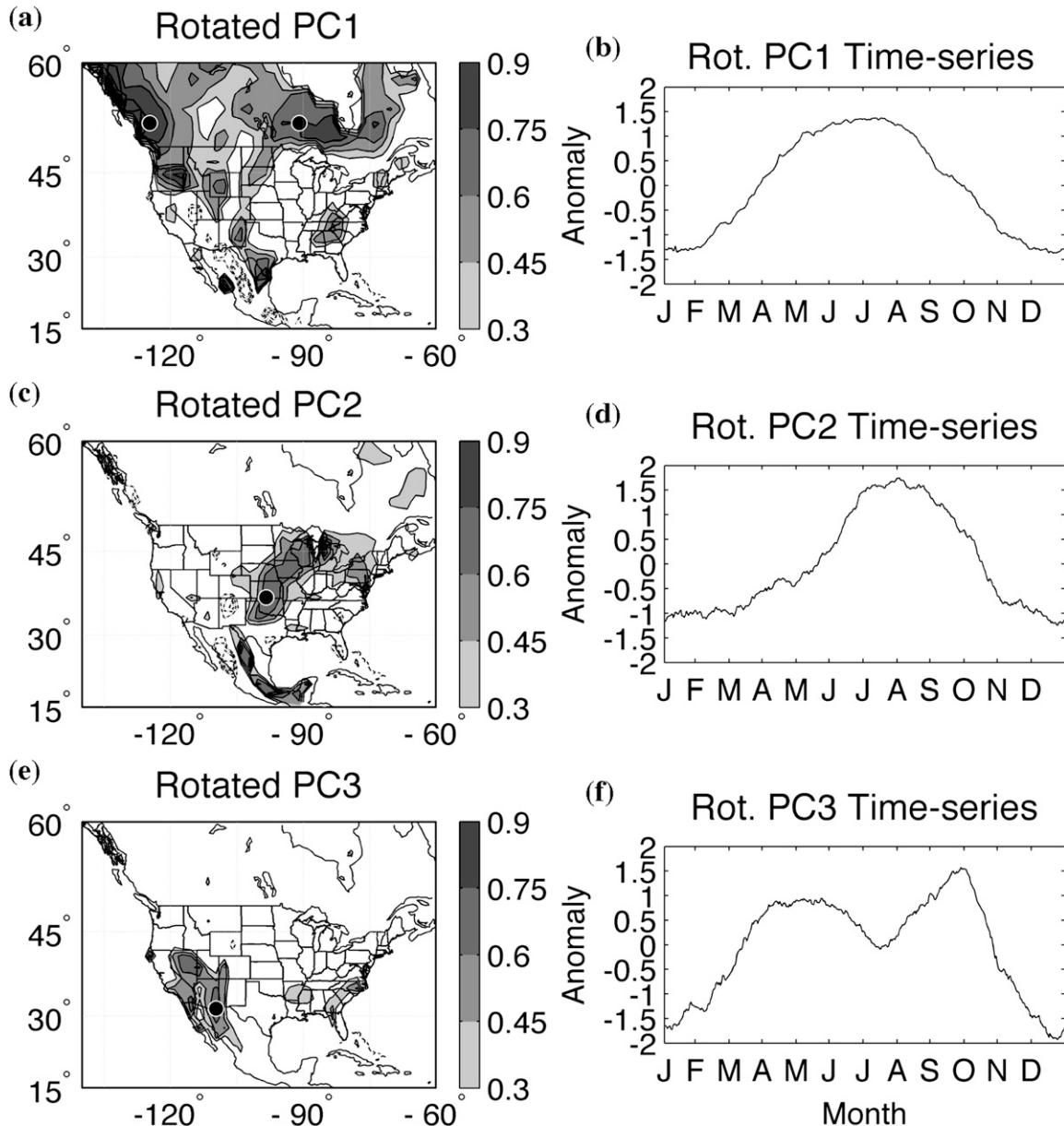


FIG. 5. (a) PC1 pattern for the climatological evolution of annual local-convergence ratio, using 30-day running mean values centered on each day of the year. Contours represent correlations with associated time series. Positive values are shaded; negative values are contoured. Minimum contour is ± 0.3 ; contour interval is 0.15. Data derived from 3-h integrations of the RII atmospheric model. Black circles represent gridpoint locations analyzed in more detail. (b) Daily evolution of PC pattern shown in (a). Time series represents normalized anomaly of 30-day running mean local-convergence ratio centered on given day of the year. (c),(d) As in (a),(b), but for rotated PC2 pattern. (e),(f) As in (a),(b), but for rotated PC3 pattern.

continental interior (Ruane and Roads 2008), as suggested here.

At the same time, there does appear to be a significant contribution to early fall precipitation by moisture-flux convergence from outside the region. The minimum and maximum values, across the three years, however, show a relatively large spread during this time. Examination of the values during individual years indicates that this

spread is mainly the result of a shift in the timing of the increased horizontal moisture-flux convergence; during 2002 increases start around August and last through the beginning of September, while in 2003 the increases start around mid-September and last through mid-October. During 2004, the increases are centered on September, as seen in Fig. 7, and also are larger than during the other two years (by about a factor of 2).

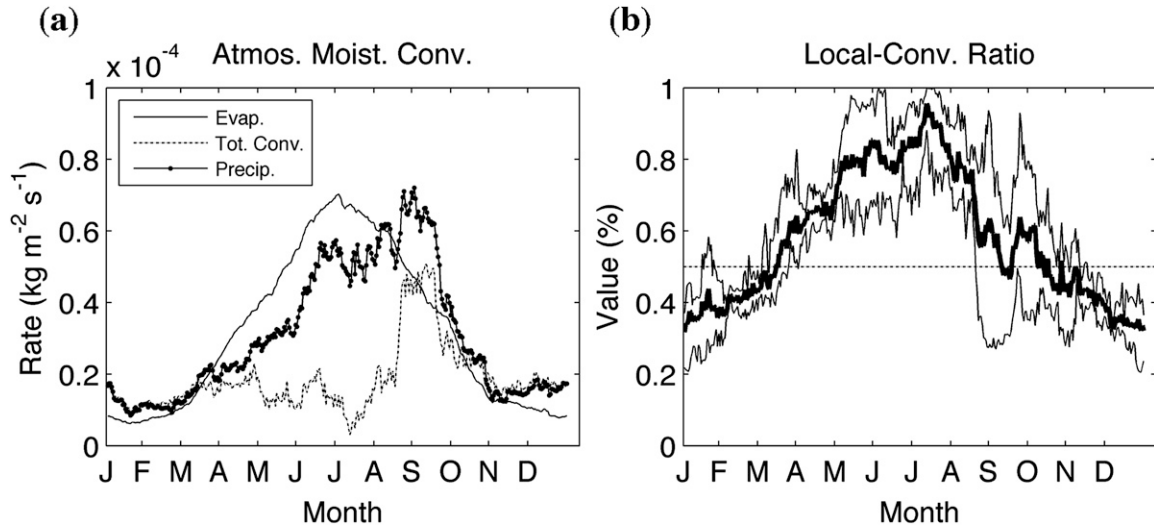


FIG. 6. (a) Climatological 30-day running mean of E (solid line), χ (dashed line), and P (dots) for central Canada site ($\text{kg m}^2 \text{s}^{-1}$; see Fig. 5a). Here, 30-day running means calculated as the box average centered on the given day; climatological values represent the average over the three simulation years. Data derived from 3-h integrations of the RII atmospheric model. (b) Climatological 30-day running mean of local-convergence ratio, λ , for central Canada site. Mean value over 3-yr period shown as thick solid line; maximum and minimum values for a given Julian day shown by thin solid lines.

To examine further the total moisture-flux convergence term during the fall peak, we plot the vertical profiles of mean horizontal moisture-flux convergence for the September period (Fig. 8), when the total moisture-flux convergence term reaches its maximum. This figure indicates that low-level horizontal moisture-

flux convergence contributes to the enhanced total moisture-flux convergence during this time. As before, there are year-to-year differences in the profiles, which are partly the result of year-to-year shifts in the timing of the late-summer/early-fall low-level horizontal moisture flux convergence. Although this feature is persistent in all three years, it is most prevalent during 2003 and 2004 and weaker during 2002. Geographic plots of the vertically integrated moisture fluxes for September (not shown) indicate that increased moisture fluxes from the Great Plains east of the Rocky Mountain plateau extend into central Canada during this time, suggesting that the enhanced low-level convergence, and increased precipitation, is associated with a northward extension of relatively moist air into the region.

Next, we turn to the northwestern coastal region and perform similar analyses as in Figs. 6–8; results are

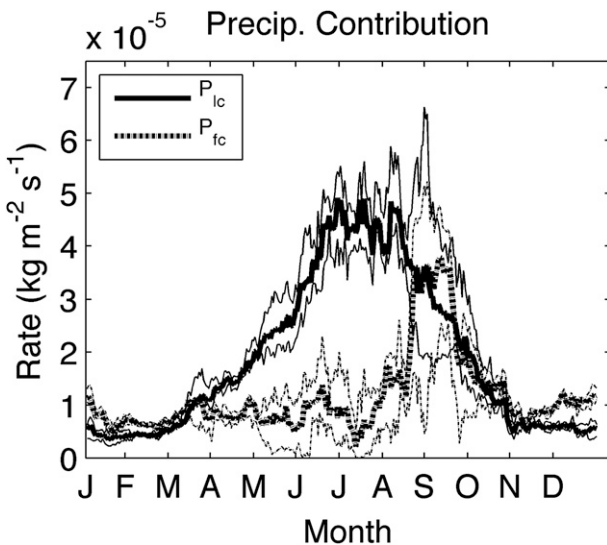


FIG. 7. Contributions of evaporation (P_{1c} , solid line) and total moisture-flux convergence (P_{fc} , dashed line) to 30-day running mean precipitation rates over the central Canada site ($\text{kg m}^2 \text{s}^{-1}$). (See text for details on calculating P_{1c} and P_{fc} .) Mean value over 3-yr period given by thick lines; maximum and minimum values for a given Julian day shown by thin lines.

TABLE 1. Contributions of evaporation to annual precipitation rates. The first column gives an estimate of the 30-day running mean local-convergence ratio, averaged over the calendar year, at each of the locations in Fig. 5. The second column is calculated by multiplying the 30-day running mean local-convergence ratio by the 30-day running mean precipitation amount and then averaging over the calendar year and normalizing by the average 30-day running mean precipitation for that location.

Location	Average λ (Jan–Dec)	Annual contribution
Central Canada	0.58	0.65
Northwest coast	0.36	0.35
Great Plains	0.54	0.59
Northwest Mexico	0.46	0.46

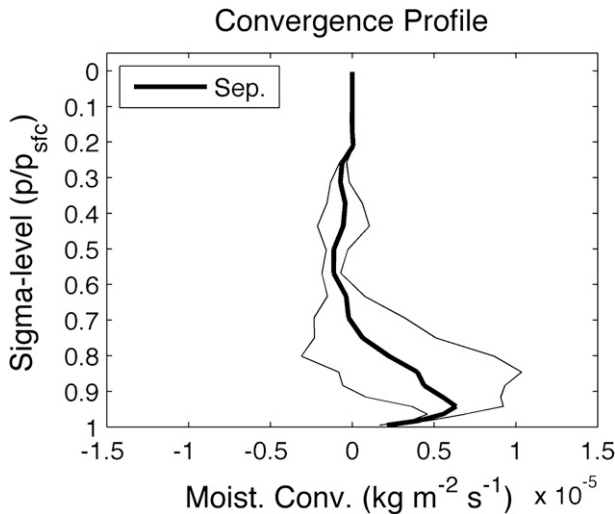


FIG. 8. Climatological profile of horizontal moisture-flux convergence/divergence for central Canada site. Horizontal axis is horizontal moisture flux convergence/divergence ($\text{kg m}^{-2} \text{s}^{-1}$) with positive values indicating moisture flux convergence; vertical axis is sigma-level $\sigma = p/p_s$. Mean value calculated as average of 30-day running means during September. Climatological value over 3-yr period shown as thick line; maximum and minimum values for a given sigma level shown by thin lines.

presented in Fig. 9. Overall, the hydrologic terms (Fig. 9a) indicate that evaporation is moderated in this region compared with the central Canada site; there is a less-dramatic increase in spring, a maximum during early and midsummer, and a decrease in fall, leading to minima during late fall and winter. In contrast, the total moisture-flux convergence term peaks during fall and early winter and then decreases during spring and summer. Despite the strong seasonal evolution of the two convergence terms (i.e., evaporation and total moisture flux convergence), precipitation remains fairly constant throughout the year. In these regions there appears to be an offsetting seasonal balance in the contribution of evaporation and moisture-flux convergence to the seasonal precipitation rates. This balance is captured by the evolution of the local-convergence ratio (Fig. 9b), which indicates that spring and summer precipitation is supported predominantly by local evaporation. During fall and early winter, however, precipitation is supported predominantly by moisture-flux convergence.

Unlike in the central Canada site, the values of P_{lc} and P_{fc} indicate substantial contributions from both over the course of the year (Fig. 9c). As would be expected from the seasonal evolution of the hydrologic components, the local contribution to precipitation (P_{lc}) peaks in midsummer, whereas the remote contribution to precipitation (P_{fc}) peaks in fall and winter, when the

region is more influenced by synoptic-type storms coming off the Pacific. Looking at the overall contribution of each to the total annual precipitation (Table 1), we find that nearly two-thirds of the precipitation is generated via moisture-flux convergence into the region, with only about a third being generated via local evaporation. These results are supported by studies examining the column-integrated water cycle, which also find that vapor flux convergence supplies much of the moisture for annual precipitation along the western coast of Canada (e.g., Ruane and Roads 2008).

To further examine the evolution of this total moisture-flux convergence, vertical plots of the horizontal moisture-flux convergence for the northwest coastal grid point are plotted for the October–December period, when the total moisture-flux convergence term is near its peak, and for the May–July period, when the term is near its nadir (Fig. 9d). During both periods, the moisture-flux convergence is occurring aloft; this vertical pattern is present both during precipitating periods as well as nonprecipitating periods (not shown). However, this figure indicates that the enhanced total moisture-flux convergence value—and the accompanying increase in P_{fc} —during late fall/early winter is related to a significant enhancement of this midlevel convergence, most likely associated with enhanced synoptic storm activity during this time period.

c. Second rotated principal component pattern

To represent the seasonal evolution of the hydrologic components and local-generation ratios associated with the second spatial pattern (rotated PC2), we choose a grid point over the central United States (see Fig. 5c). As with the previous two locations, the seasonal evolution of the evaporation peaks in the summer months and shows a minimum in winter (Fig. 10a). The total moisture-flux convergence term also begins to increase in spring. It reaches a peak in late spring and then decreases in early summer and stays relatively low throughout the summer season. In contrast, the precipitation term increases at the same time as both the evaporation and moisture-flux convergence and then remains high through most of the summer into early fall before decreasing again. From this figure, it appears that although the springtime increase in precipitation in this region is balanced in part by moisture-flux convergence, the summertime persistence of this precipitation is balanced predominantly by local evaporation.

This result is mirrored in the seasonal evolution of the local-convergence ratio (Fig. 10b). During fall and winter, the ratio is low principally because of the low evaporation rates during this time of year. However, the ratio remains low throughout spring because the total

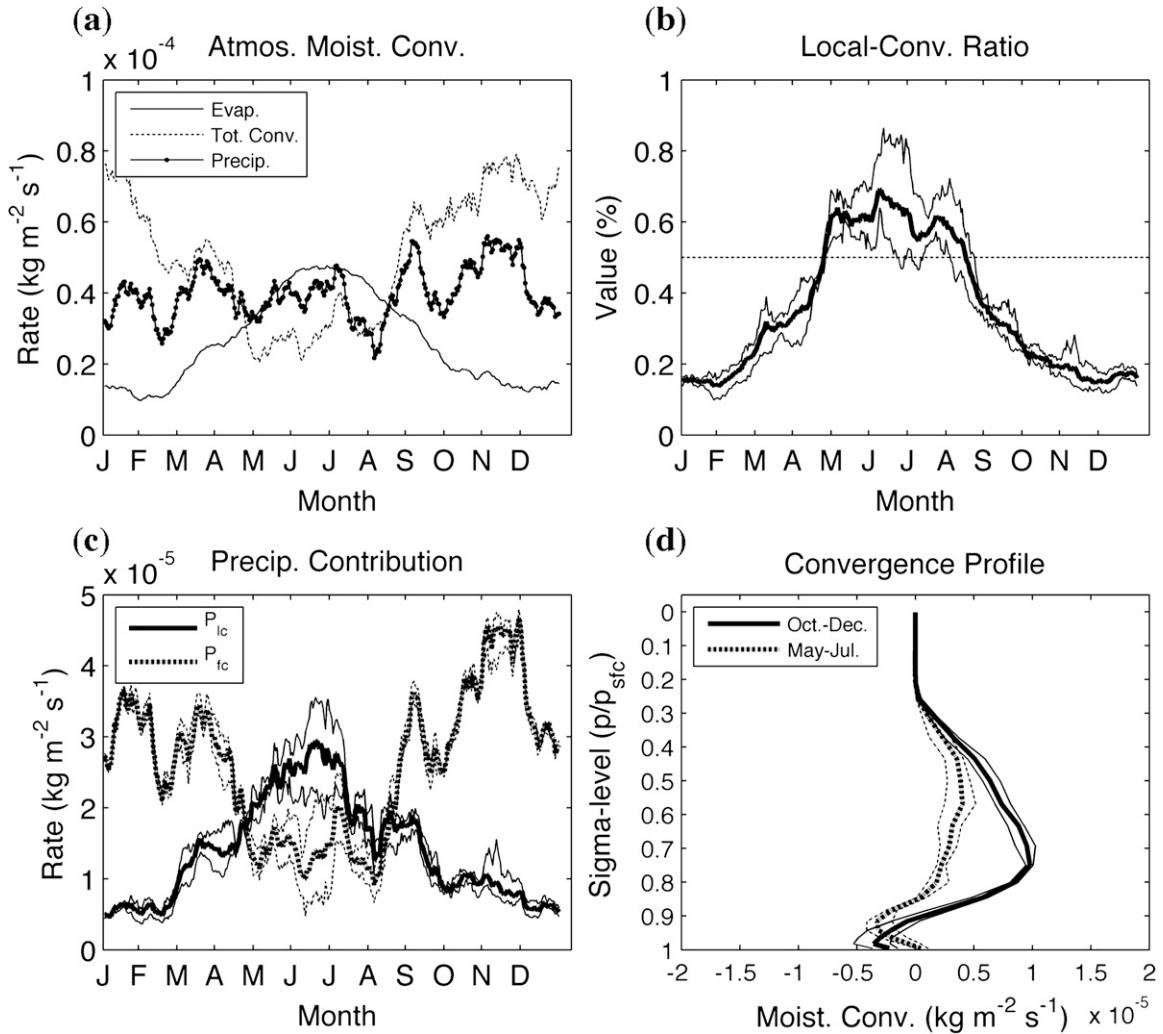


FIG. 9. As in Figs. 6–8 but for northwest coastal site (see Fig. 5a).

moisture-flux convergence increases concurrent with the evaporation. In fact, during this time about half of the precipitation is balanced by moisture-flux convergence and about half by local evaporation. However, during summer the local-convergence ratio increases as the total moisture-flux convergence term collapses, indicating again that summertime precipitation is balanced mainly by evaporative convergence within the region.

If we examine the local and remote contributions to total precipitation (P_{lc} and P_{fc} , Fig. 10c), we find that while moisture-flux convergence from outside the region is important during the initial springtime increase (as suggested before), the annual precipitation amount, which is dominated by the rainfall rates during summer, is balanced predominantly by evaporative contributions. When looking at the overall contributions of each (Table 1), we find that about 60% of the annual pre-

cipitation is generated via local evaporation, slightly larger than the annual mean value of the local-convergence ratio itself.

As discussed, the relatively low contribution of moisture-flux convergence to the annual precipitation budget is principally due to the collapse of the total moisture-flux convergence values during summer, when precipitation is a maximum. Hence, it is of interest to examine further the total moisture-flux convergence term during spring, when it peaks, and in summer, after it collapses. To do so, we plot the vertical profiles of mean horizontal moisture-flux convergence for the period 15 April–15 June (the period of maximum total moisture flux convergence seen in Fig. 10a) and separately for the period 1 July–1 August (Fig. 10d). During the mid- and late-spring period, there is substantial low-level convergence of moisture associated with the intensification of the Great Plains low-level jet during this

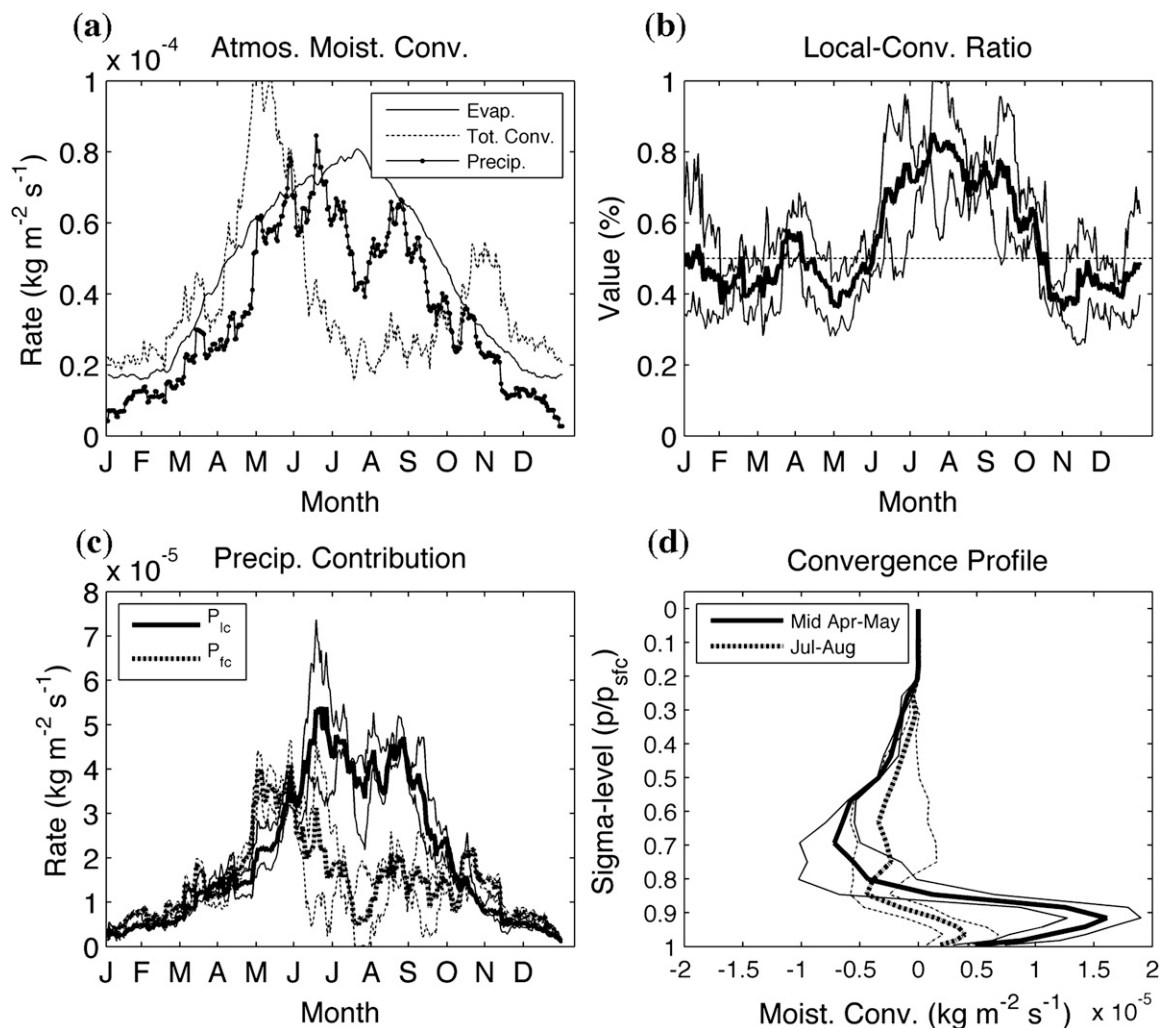


FIG. 10. As in Figs. 6–8 but for Great Plains site (see Fig. 5c).

time (Higgins 1996). Ruane and Roads (2007a, 2008) demonstrated that this low-level jet moisture convergence is related to propagating diurnal thunderstorms as they move across the Great Plains in the afternoon and arrive at the Great Lakes in the early morning hours (as observed by Carbone et al. 2002).

During June and July, this low-level moisture-flux convergence decreases substantially. However, enhanced vertically integrated moisture fluxes at this grid point are maintained throughout the summertime period (see Fig. 4 from Anderson et al. 2008). Hence, although the low-level jet activity may continue to supply precipitable water to the region during summer, the lack of moisture-flux convergence associated with this jet activity indicates it does not necessarily support the summertime precipitation budget. Instead, the precipitation budget during this time is predominantly supported by local evaporation, again in agreement with

results derived from the column-integrated water cycle (Ruane and Roads 2008).

d. Third rotated principal component pattern

Finally, to represent the seasonal evolution of the hydrologic components and local-generation ratio for the third spatial pattern (rotated PC3), we choose a grid point over northwestern Mexico (see Fig. 5e). With regard to the hydrologic components (Fig. 11a), the seasonal evolution of evaporation is not as monotonic as at the other locations, with a local minimum occurring during late spring when rainfall is near zero. However, the peak in evaporation still occurs in late summer with minimum values during winter. The total moisture-flux convergence term is dominated by a large maximum during mid- and late-summer into early fall (July–September), which coincides with the monsoon rains

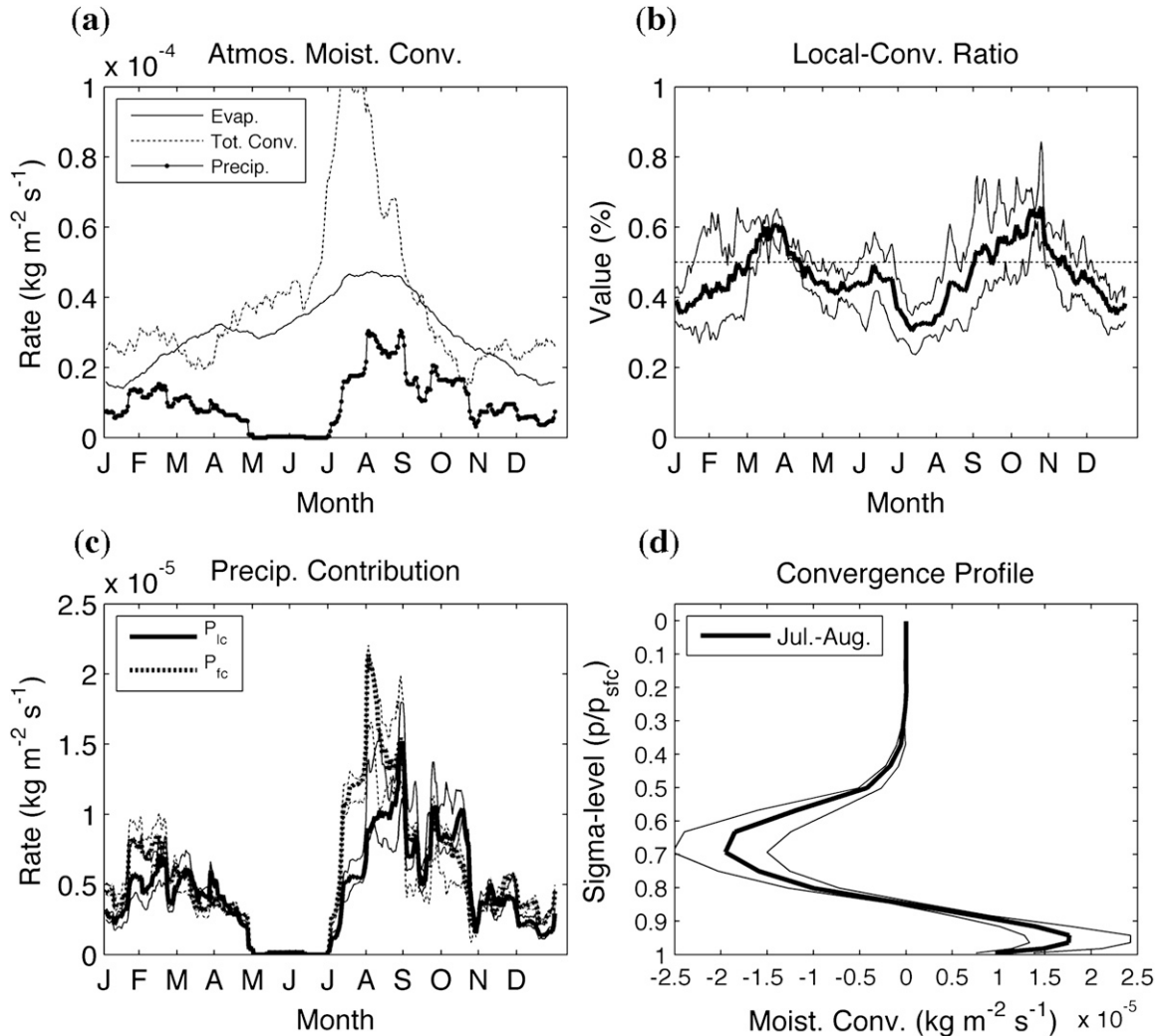


FIG. 11. As in Figs. 6–8 but for northwest Mexico site (see Fig. 5e).

in this region. These monsoon rains are seen as a maximum in the precipitation evolution during this same period. There is a second local maximum in precipitation during winter as well.

The evolution of the local-generation ratio (Fig. 11b) shows a profile similar to the time series for the rotated principal component map. There are two local maxima during spring and late fall, with minima occurring during late summer/early fall and during winter. This result suggests that moisture-flux convergence helps balance seasonal precipitation both during the rainy monsoon season and during the wintertime season. In addition, it appears that because of limited local water availability, the local convergence value is less than 0.5 through most of the year, indicating that moisture-flux convergence is an important contributor to precipitation budgets during the rest of the year as well.

Indeed, if we examine the amount of precipitation contributed by evaporation and moisture-flux convergence (P_{lc} and P_{fc}), we find that except during the early monsoon period (July–August), the values are relatively similar (Fig. 11c). During the early monsoon period, however, the moisture-flux contribution from outside the region supports about two-thirds of the rainfall. By September, though, the evaporative contribution begins to match the moisture-flux contribution, suggesting that the persistence of the monsoon rains through September and into October (see Fig. 11a) is also supported via local evaporation. Looking at the annual values, we find P_{lc} and P_{fc} contribute about equally to precipitation over the course of the year (Table 1), with slightly more being supported by moisture-flux convergence from outside the region as a result of the enhancement of summertime rainfall by moisture-flux convergence.

Given the magnitude of the total moisture-flux convergence value during summertime (July–August; Fig. 11a), it is of interest to further examine vertical profiles of the horizontal moisture-flux convergence that contributes to it (Fig. 11d). Overall, during this time there is significant low-level moisture flux convergence into the region and upper-level moisture-flux divergence out of the region. These profiles are in agreement with previous studies investigating the climatological hydrologic balances for this region (Schmitz and Mullen, 1996; Berbery, 2001; Anderson et al. 2004), in which enhanced summertime rainfall is supported by intensified moisture-flux convergence associated with continental-scale North American monsoon circulations. During the winter season (November–March), horizontal moisture-flux convergence profiles are similar to the ones found over the northwest coastal region—comprising low-level moisture-flux divergence and upper-level moisture-flux convergence (not shown)—likely associated with the interaction of synoptic storms with the surrounding mountain barriers.

4. Summary and discussion

a. Summary

We have used a new tendency-based metric for estimating the influence of evaporation upon precipitation budgets over the North American region, based upon the NCEP–DOE Reanalysis-2 model system. In general, the fractional evaporative contribution increases with evaporation itself and hence shows maximum values in spring and summer and minimum values in fall and winter. However, within this broad evolution there appears to be at least three regional spatiotemporal evolution patterns: The first, situated over the northern and western portions of the continent, shows a maximum in the evaporative contribution during spring and into summer. The second, situated over the central portion of the continent, indicates relatively low evaporative contributions during spring but maximum contributions during summer and into fall. The third, positioned over the southwestern portion of the United States and northwestern portion of Mexico, indicates minimum evaporative contributions during winter and a secondary minimum during summer.

Analysis of the hydrologic components—evaporation, total moisture-flux convergence, and precipitation—at representative grid points allows us to further analyze this seasonal evolution. Over the northern portion of the domain, evaporative contributions to precipitation increase with evaporation itself, particularly in spring and summer. However, during fall the fractional contribution decreases sharply in association with an in-

crease in low-level moisture flux convergence into the region; this low-level moisture flux convergence, in turn, is related to an extension of northward meridional moisture transport into the region. In contrast, over the western coast of the continent, the drop-off in evaporative contribution to precipitation in fall is related to an increase in total moisture-flux convergence that persists through the winter, as the region is influenced by the passage of synoptic storm systems coming off the Pacific Ocean.

Over the central portion of the continent, the fractional contribution of evaporation to precipitation does not begin until summer but then persists into fall. At these locations, there is an increase in evaporation during spring; however, there is a corresponding increase in low-level moisture-flux convergence as well, both of which balance an increase in precipitation during this time. In summer, the low-level moisture flux convergence term decreases substantially; during this time, the persistence of precipitation is balanced almost entirely by evaporation. In contrast, over southwestern North America, there is actually a decrease in the evaporative contribution to precipitation during summer. In these regions, increases in precipitation during summer are balanced by an increase in low-level moisture flux convergence into the region, associated with the low-level monsoon circulations that form over this region during this time.

It is important to note that these results are based upon numerical model simulations taken from the NCEP–DOE Reanalysis-2 model system. Previously, Roads et al. (2002) have found differences in the model-generated and observed annual means and seasonal cycles of precipitation. However, Ruane and Roads (2008) find large-scale agreement between the NCEP–DOE Reanalysis-2 model intra-annual, intraseasonal, and diurnal water cycle balances (e.g., evaporation, vertically integrated moisture-flux convergence, and vertically integrated moisture tendency) even when observed precipitation is substituted for the modeled fields, suggesting that the seasonal evolutions of evaporation, moisture-flux convergence, and their relative contributions to precipitation (which does not depend upon precipitation itself)—as found in this study—may also be representative of those found in the real system. In addition, there exist intermodel differences in the annual means and seasonal cycles of hydrologic quantities such as evaporation and precipitation (Betts et al. 2006; Szeto et al. 2008; Ruane and Roads 2007b). Unfortunately, we cannot compare the results here with those from other modeling systems [for instance, with the European Centre for Medium-Range Weather Forecasts (ECMWF) reanalysis model], because retroactively generating the data for this analysis is computationally intensive (requiring rerunning the

reanalysis models with additional code designed to archive the sigma-level moisture-budget terms at 3-h intervals). However, future work will focus on evaluating these results using different modeling systems as well as observationally based products.

b. Discussion

In the introduction, it was highlighted that regional precipitation-recycling ratios (as well as the local-convergence ratio discussed here) may be able to provide information about the enhancement/reduction of precipitation as a result of land surface/precipitation interactions (Brubaker et al. 1993; Burde and Zangvil 2001; Bosilovich 2002). For instance, during spring and summer local-convergence ratios indicate that precipitation across most of the western interior of the continent and the eastern third is balanced predominantly by local evaporation (see Figs. 1a,b). This result suggests that seasonal-mean precipitation rates during this time depend primarily on the local availability of water, especially over the interior lowlands to the east of the Great Plains.

Over the western Great Plains, however, there is a local minimum in the local-convergence ratio during spring and summer, compared with surrounding areas (see Fig. 1b), indicating that precipitation in these regions may be affected by changes in large-scale dynamics of the system, as well as by local water availability. Conversely, previous studies have shown that these regions are ones in which the local land surface conditions have the largest effects upon precipitation generation (Koster et al. 2004; Dirmeyer, et al. 2006; Guo et al. 2006).

How should we reconcile these two results? As pointed out by Koster et al. (2004) and Guo et al. (2006), for regional precipitation to be sensitive to land surface changes, two criteria must be met: 1) the evaporative fluxes must be sensitive to changes in underlying soil moisture; and 2) precipitation must be sensitive to changes in the evaporative fluxes. These two criteria are most often met in semiarid regions, such as the western Great Plains (Koster et al. 2004; Dirmeyer et al. 2006). However, during summer, precipitation's response to evaporation is driven by subsequent changes in the thermodynamic structure of the atmosphere, not necessarily by the evaporative fluxes themselves. Instead, soil moisture-induced increases in evaporation can enhance regional convective instability and hence lead to increased precipitation (Betts et al. 1996; Eltahir 1998; Pal and Eltahir 2001; Barros and Hwu 2002; Small and Kurc 2003; Guo et al. 2006); in addition, enhanced evaporation can modify the low-level and upper-level temperature and pressure patterns, thereby enhancing

the large-scale moisture fluxes and moisture-flux convergence fields, leading to increased precipitation (Namias 1991; Fennessy and Shukla 1999; Kanamitsu and Mo 2003; Xu et al. 2004; Li and Fu 2004; Anderson et al. 2006).

On the basis of our results, and those of Koster et al. (2004), we *hypothesize* that land-atmosphere coupling strength is not only dependent upon the high response of evaporation to soil moisture variations and high variability in evaporation itself (Guo et al. 2006) but also upon relatively large moisture-flux convergence from outside the region (represented here by relatively low local-convergence ratios). With an ample convergence of external moisture, precipitation can respond more readily to (indirect) soil moisture-induced variations in evaporation, as described earlier. Without this external support of moisture convergence, soil moisture-induced variations in evaporation may produce the necessary changes in the thermodynamic and dynamic structure of the atmosphere needed to initiate precipitation, but the lack of continuous convergence of external moisture reduces any subsequent precipitation response. Comparison of global maps of the local-convergence ratio (Anderson et al. 2008) with maps of strong coupling between soil moisture and precipitation (Koster et al. 2004) indicates minima (maxima) in the local-convergence ratios (coupling) over the central United States, India, and central Africa, supporting the hypothesized relation between the two. However, further investigation of this hypothesis will require computing the local-convergence ratios found in each of the model systems used for soil moisture sensitivity studies and then comparing the geographic structure of the local-convergence ratio with the soil-moisture "hot spots" within the same model system, something that is beyond the scope of this paper. Similarly, this type of investigation may also help identify regions in which *decreases* in evaporation contribute to enhanced precipitation (again, by indirectly enhancing thermally driven convergence of external moisture), leading to sustained oscillatory behavior in the hydrologic cycle (e.g., Abbot and Emanuel 2007).

Acknowledgments. This research was funded in part by NOAA Cooperative Agreements NA17RJ1231 and NA16GP1622. The views expressed herein are those of the authors and do not necessarily reflect the views of NOAA. Dr. Anderson's research was also supported by a Visiting Scientist appointment to the Grantham Institute for Climate Change, administered by Imperial College of Science, Technology, and Medicine. Dr. Ruane's research was supported by an appointment to the NASA Postdoctoral Program at the NASA Goddard Institute

for Space Studies, administered by Oak Ridge Associated Universities through a contract with NASA. We also extend our appreciation to the three anonymous reviewers for all their insightful and constructive comments.

REFERENCES

- Abbot, D. S., and K. A. Emanuel, 2007: A tropical and subtropical land–sea–atmosphere drought oscillation mechanism. *J. Atmos. Sci.*, **64**, 4458–4466.
- Anderson, B. T., and J. O. Roads, 2001: Summertime moisture divergence over the southwestern US and northwestern Mexico. *Geophys. Res. Lett.*, **28**, 1973–1976.
- , H. Kanamaru, and J. O. Roads, 2004: The summertime atmospheric hydrologic cycle over the southwestern United States. *J. Hydrometeorol.*, **5**, 679–692.
- , —, and —, 2006: Variations in the summertime atmospheric hydrologic cycle associated with seasonal precipitation anomalies over the southwestern United States. *J. Hydrometeorol.*, **7**, 788–807.
- , G. Salvucci, A. Ruane, M. Kanamitsu, and J. O. Roads, 2008: A new metric for estimating the influence of evaporation upon seasonal precipitation rates. *J. Hydrometeorol.*, **9**, 576–588.
- Barros, A. P., and W. J. Hwu, 2002: A study of land-atmosphere interactions during summertime rainfall using a mesoscale model. *J. Geophys. Res.*, **107**, 4227, doi:10.1029/2000JD000254.
- Berbery, E. H., 2001: Mesoscale moisture analysis of the North American monsoon. *J. Climate*, **14**, 121–137.
- Betts, A. K., and Coauthors, 1996: The land surface-atmosphere interaction: A review based on observational and global modeling perspectives. *J. Geophys. Res.*, **101**, 7209–7225.
- , M. Zhao, P. A. Dirmeyer, and A. C. M. Beljaars, 2006: Comparison of ERA40 and NCEP/DOE near-surface data sets with other ISLSCP-II data sets. *J. Geophys. Res.*, **111**, D22S04, doi:10.1029/2006JD007174.
- Bosilovich, M. G., 2002: On the vertical distribution of local and remote sources for precipitation. *Meteor. Atmos. Phys.*, **80**, 31–41.
- , and S. D. Schubert, 2002: Water vapor tracers as diagnostics of the regional hydrologic cycle. *J. Hydrometeorol.*, **3**, 149–165.
- Brubaker, K. L., D. Entekhabi, and P. S. Eagleson, 1993: Estimation of continental precipitation recycling. *J. Climate*, **6**, 1077–1089.
- Burde, G. I., and A. Zangvil, 2001: The estimation of regional precipitation recycling. Part I: Review of recycling models. *J. Climate*, **14**, 2497–2508.
- Carbone, R. E., J. D. Tuttle, D. A. Ahijevych, and S. B. Trier, 2002: Inferences of predictability associated with warm season precipitation episodes. *J. Atmos. Sci.*, **59**, 2033–2056.
- Chen, S.-C., C. L. Norris, and J. O. Roads, 1996: Balancing the atmospheric hydrologic budget. *J. Geophys. Res.*, **101**, 7341–7358.
- Comrie, A. C., and E. C. Glenn, 1998: Principal components-based regionalization of precipitation regimes across the southwest United States and northern Mexico, with an application to monsoon precipitation variability. *Climate Res.*, **10**, 201–215.
- Dirmeyer, P. A., and K. L. Brubaker, 2007: Characterization of the global hydrologic cycle from a back-trajectory analysis of atmospheric water vapor. *J. Hydrometeorol.*, **8**, 20–37.
- , R. D. Koster, and Z. Guo, 2006: Do global models properly represent the feedback between land and atmosphere? *J. Hydrometeorol.*, **7**, 1177–1198.
- Douglas, M. W., R. A. Maddox, and K. Howard, 1993: The Mexican monsoon. *J. Climate*, **6**, 1665–1677.
- Ebisuzaki, W., 1997: A method to estimate the statistical significance of a correlation when the data are serially correlated. *J. Climate*, **10**, 2147–2153.
- Eltahir, E. A. B., 1998: A soil moisture–rainfall feedback mechanism, 1. Theory and observations. *Water Resour. Res.*, **34**, 765–776.
- Fennessy, M. J., and J. Shukla, 1999: Impact of initial soil wetness on seasonal atmospheric prediction. *J. Climate*, **12**, 3167–3180.
- Guo, Z., and Coauthors, 2006: GLACE: The global land–atmosphere coupling experiment. Part II: Analysis. *J. Hydrometeorol.*, **7**, 611–625.
- Higgins, R. W., 1996: The moisture budget of the central United States in spring as evaluated in the NCEP/NCAR and the NASA/DAO reanalyses. *Mon. Wea. Rev.*, **124**, 939–963.
- , Y. Yao, and X. L. Wang, 1997a: Influence of the North American monsoon system on the United States summer precipitation regime. *J. Climate*, **10**, 2600–2622.
- , —, E. S. Yarosh, J. E. Janowiak, and K. C. Mo, 1997b: Influence of the Great Plains low-level jet on summertime precipitation and moisture transport over the central United States. *J. Climate*, **10**, 481–507.
- Higgins, W., and Coauthors, 2006: The NAME 2004 field campaign and modeling strategy. *Bull. Amer. Meteor. Soc.*, **87**, 79–94.
- Hurrell, J. W., and H. van Loon, 1997: Decadal variations in climate associated with the North Atlantic Oscillation. *Climatic Change*, **36**, 301–326.
- Kanamitsu, M., 2003: Atmospheric water budget viewed from three-component exchange diagram. *Proc. IUGG XXIII General Assembly*, Sapporo, Japan, International Union of Geodesy and Geophysics.
- , and K. C. Mo, 2003: Dynamical effect of land surface processes on summer precipitation over the southwestern United States. *J. Climate*, **16**, 496–509.
- , W. Ebisuzaki, J. Woollen, S. K. Yang, J. J. Hnilo, M. Fiorino, and G. L. Potter, 2002: NCEP–DOE AMIP-II reanalysis (R-2). *Bull. Amer. Meteor. Soc.*, **83**, 1631–1643.
- Koster, R. D., and Coauthors, 2004: Regions of strong coupling between soil moisture and precipitation. *Science*, **305**, 1138–1140.
- Lawford, R., and Coauthors, 2006: U.S. contributions to the CEOP. *Bull. Amer. Meteor. Soc.*, **87**, 927–939.
- Li, W., and R. Fu, 2004: Transition of the large-scale atmospheric and land surface conditions from the dry to the wet season over Amazonia as diagnosed by the ECMWF re-analysis. *J. Climate*, **17**, 2637–2651.
- Maurer, E. P., G. M. O'Donnell, D. P. Lettenmaier, and J. O. Roads, 2001: Evaluation of the land surface water budget in NCEP/NCAR and NCEP/DOE reanalyses using an off-line hydrologic model. *J. Geophys. Res.*, **106**, 17 841–17 862.
- Namias, J., 1991: Spring and summer 1988 drought over the contiguous United States—causes and prediction. *J. Climate*, **4**, 54–65.
- Pal, J. S., and E. A. B. Eltahir, 2001: Pathways relating soil moisture conditions to future summer rainfall within a model of the land–atmosphere system. *J. Climate*, **14**, 1227–1242.
- Rasmusson, E. M., 1968: Atmospheric water vapor transport and the water balance of North America II. Large-scale water balance investigations. *Mon. Wea. Rev.*, **96**, 720–734.
- Richman, M. B., 1986: Rotation of principal components. *J. Climatol.*, **6**, 293–335.

- Roads, J. O., and Coauthors, 1992: Global aspects of the Los Alamos general circulation model hydrologic cycle. *J. Geophys. Res.*, **97**, 10 051–10 068.
- , M. Kanamitsu, and R. Stewart, 2002: CSE water and energy budgets in the NCEP–DOE Reanalysis II. *J. Hydrometeorol.*, **3**, 227–248.
- , and Coauthors, 2003: GCIP water and energy budget synthesis (WEBS). *J. Geophys. Res.*, **108**, 8609, doi:10.1029/2002JD002583.
- Ropelewski, C. F., and M. S. Halpert, 1986: North American precipitation and temperature patterns associated with the El Niño/Southern Oscillation (ENSO). *Mon. Wea. Rev.*, **114**, 2352–2362.
- Ruane, A. C., and J. O. Roads, 2007a: The diurnal cycle of water and energy over the continental United States from three reanalyses. *J. Meteor. Soc. Japan*, **85A**, 117–143.
- , and —, 2007b: 6-hour to 1-year variance of five global precipitation sets. *Earth Interactions*, **11**. [Available online at <http://EarthInteractions.org>.]
- , and —, 2008: Dominant balances and exchanges of the atmospheric water cycle in the reanalysis 2 at diurnal, annual, and intraseasonal time scales. *J. Climate*, **21**, 3951–3966.
- Schmitz, J. T., and S. L. Mullen, 1996: Water vapor transport associated with the summertime North American monsoon as depicted by ECMWF analyses. *J. Climate*, **9**, 1621–1634.
- Small, E. E., and S. A. Kurc, 2003: Tight coupling between soil moisture and the surface radiation budget in semiarid environments: Implications for land-atmosphere interactions. *Water Resour. Res.*, **39**, 1278.
- Starr, V. P., and J. P. Peixoto, 1958: On the global balance of water vapor and the hydrology of deserts. *Tellus*, **10**, 189–194.
- Stewart, R. E., and Coauthors, 1998: The Mackenzie GEWEX study: The water and energy cycles of a major North American river basin. *Bull. Amer. Meteor. Soc.*, **79**, 2665–2683.
- Szeto, K. K., and Coauthors, 2008: The MAGS water and energy budget study. *J. Hydrometeorol.*, **9**, 96–115.
- Trenberth, K. E., 1999: Atmospheric moisture recycling: Role of advection and local evaporation. *J. Climate*, **12**, 1368–1381.
- Wallace, J. M., 1975: Diurnal variations in precipitation and thunderstorm frequency over the conterminous United States. *Mon. Wea. Rev.*, **103**, 406–419.
- Xu, J., and Coauthors, 2004: Model climatology of the North American monsoon onset period during 1980–2001. *J. Climate*, **17**, 3892–3906.